Editors' Suggestion

Anomalous bulk-edge correspondence in continuous media

C. Tauber,[1,*] P. Delplace,[2] and A. Venaille[2]

[1]*Institute for Theoretical Physics, ETH Zurich, Wolfgang-Pauli-Str. 27, CH-8093 Zurich, Switzerland*

[2]*Univ Lyon, Ens de Lyon, Univ Claude Bernard, CNRS, Laboratoire de Physique, F-69342 Lyon, France*

(Received 13 March 2019; accepted 13 January 2020; published 11 February 2020)

Topology plays an increasing role in physics beyond the realm of topological insulators in condensed mater. From geophysical fluids to active matter, acoustics or photonics, a growing family of systems presents topologically protected chiral edge modes. The number of such modes should coincide with the bulk topological invariant (e.g., Chern number) defined for a sample without boundary, in agreement with the bulk-edge correspondence. However, this is not always the case when dealing with continuous media where there is no small scale cutoff. The number of edge modes actually depends on the boundary condition, even when the bulk is properly regularized, showing an apparent paradox where the bulk-edge correspondence is violated. In this paper, we solve this paradox by showing that the anomaly is due to *ghost* edge modes hidden in the asymptotic part of the spectrum, which have a signature at finite frequency both in the local density of states and in a channel geometry. We provide a general formalism based on scattering theory to detect all edge modes properly, so that the bulk-edge correspondence is restored in a broader sense, implying in particular that chiral edge modes are not necessarily topological, and conversely. Our approach is illustrated through the odd-viscous shallow-water model and the massive Dirac Hamiltonian.

DOI: 10.1103/PhysRevResearch.2.013147

I. INTRODUCTION

Tools from topology are central to our understanding of a variety of physical phenomena [1], from quantized vortices in superfluids [2–4], to defects in ordered media [5–7], or to the description vorticity knots in classical fluids [8], among other applications. Over the last decades, topology has also played a central role in the study of waves, starting with wavefront dislocations [9] and culminating with the now celebrated bulk-edge correspondence [10,11] inherited from the quantum Hall effect. Such a correspondence is a hallmark of topology in physics which states that, when there exists a topological number associated to an infinite and gapped system (bulk picture), then topologically protected edge modes appear in a sample with a boundary (edge picture) and vice versa. These modes are confined near the boundary, robust to many perturbations and their number coincide with the bulk topological quantity.

It was first realized in quantum Hall effect that both bulk and edge pictures were associated to topological quantities [12–14], which actually coincide [10,11]. It was then widely expanded through the field of topological insulators [15], where the bulk-edge correspondence was studied and proved in systems with various dimensions and symmetries [16–20], in presence of (strong) disorder [21–24], or for periodically driven (Floquet) systems [25–28].

The aim of this paper is to address the relevance of bulk-edge correspondence for continuous media, focusing and two emblematic physical systems. In the context of condensed matter the bulk-edge correspondence usually focuses on lattice models thank to the tight-binding approximation. However this problem was somehow overlooked in continuous models, namely beyond this approximation or when there is no underlying lattice structure. Apart from continuous electronic models, e.g., the Landau Hamiltonian, topology has also appeared in virtually all fields of physics, from superfluids [29] to photonics [30–34] or molecular spectra [35], among others. These ideas have then been applied to the realm of classical fluid and solid mechanics, including elasticity [36–38], acoustics [39–42], geophysical and astrophysical flows [43,44], plasma [45–49], or active matter [50–52]. There, a continuous medium description is natural.

One example is the two-dimensional shallow-water model describing Earth atmospheric and oceanic layers [43,53], and its formal analogs encountered in active matter and plasma physics [52], as well as in optical systems [54]. It appears as a paradigmatic (spin 1) three band model, by analogy with the celebrated (spin 1/2) Dirac Hamiltonian [29]. In the context of geophysical fluids, the topology of the shallow-water model was recently revealed. Due to the sign change of the Coriolis force, the existence of unidirectional waves propagating near the equator could be interpreted as topologically protected [43]. More recently it was shown that a topological (Chern) number can be assigned to the bulk problem for this flow, up to a regularization by an odd-viscous term [52,53]. Indeed, in contrast to condensed matter where quasimomenta live on a compact torus (Brillouin zone), the momentum

*tauberc@phys.ethz.ch

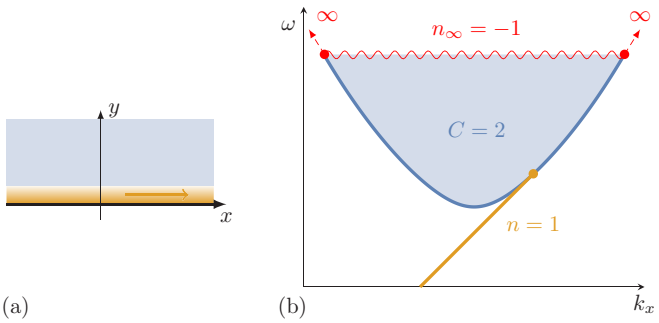

FIG. 1. (a) Continuous model with a sharp boundary. (b) Typical spectrum: the delocalized bulk modes form a band (in blue) that is gapped below but unbounded above. It has a topological (Chern) number C. The gapped region may host n edge modes (in orange) that are confined near the boundary and unidirectional. Although topological, this number apparently depends on the boundary condition. However the bulk-edge correspondence $C = n - n_\infty$ is always satisfied if we take into account possible ghost modes at infinity (in red).

(or the wave number) is usually unbounded in continuous models in the absence of any cutoff and has to be properly regularized. In this way, as in condensed matter, a meaningful bulk topological number can be defined that is expected to rule the bulk-boundary correspondence in continuous media and thus predict the number of chiral edge modes.

However, as we shall see, the regularization of the bulk does not implies the same for the edge problem. Indeed, in the shallow water model, we observe that the number of edge modes depends on the boundary condition, be it with odd-viscous terms [53], or without it [55]. This looks suspicious compared to the expected topological nature of these modes in the presence of odd viscosity, and raises the apparent paradox of a violation of the bulk-edge correspondence. This anomaly is not restricted to the shallow-water model and was actually already noticed in other two-dimensional continuous models, e.g., in the valley quantum Hall effect [56] or compressible stratified fluids [57], that are both effectively well described by a Dirac Hamiltonian.

In this paper, we propose a solution to this paradox and restore the bulk-edge correspondence for continuous models with a sharp boundary. The crucial observation is that in such models, neither the longitudinal momentum nor the frequency (or energy) are bounded, so that the usual way to count the edge modes might miss the asymptotic area of the spectrum, see Fig. 1. Thus we provide an alternative formalism based on scattering theory, that counts properly the usual edge modes but also allows to detect *ghost edge modes* that could be hidden at infinite frequencies in the spectrum. Applying it to several boundary conditions, we show that this is indeed the case so that the bulk-edge correspondence is restored when all the modes, including the ghost modes that are not visible in the spectrum at finite frequency and momentum, are properly taken into account, thus revealing an *anomalous bulk-boundary correspondence* for continuous media. Note that this approach works beyond the illustrative choice of the shallow-water model and applies similarly to any continuous model as long as the bulk is properly regularized, such as the compactified Dirac Hamiltonian that we also tackle at the end.

Scattering theory has been previously involved into the definition of topological quantities in tight-binding discrete models, through two independent ways. The first way was to probe the presence of edge modes of a topological sample through scattering from *outside* the sample [58–61], e.g., with external leads. The second way was to probe the edge through the scattering of bulk waves, namely *inside* the sample, at the boundary [19,62]. Our strategy is to apply the latter approach to continuous models in order to explore the asymptotic part of the spectrum, hence revealing the possible presence of ghost edge modes.

Note that a different way to study the edge problem for continuous models is to consider a confining potential or a continuous interface between two topologically distinct samples [62–66]. Such an interface is smoother than a sharp boundary and usually regularizes the problem so that there is no hidden mode at infinity. However, with a few exceptional cases, the counterpart of this approach is the loss of exact solvability. The main conclusion of this paper is that the bulk-edge correspondence for a sharp boundary is also perfectly valid as long as all edge modes, including the ones hidden at infinity, are properly taken into account.

The paper is organized as follows. In Sec. II, we present a continuous model and compute the edge spectrum for different boundary conditions, revealing an apparent anomaly. Section III discusses the bulk-edge correspondence in details in order to quantify the previous mismatch. Section IV introduces scattering theory and solves the paradox, and Sec. V discusses the physical consequences. Section VI shows the universality of this approach by applying it to the Dirac Hamiltonian. Section VII concludes and suggest several consequences of this new paradigm.

II. SHALLOW-WATER WITH ODD VISCOSITY

The two-dimensional rotating shallow-water model, linearized around a rest state in a rotating reference frame, is ruled by the following system:

$$\partial_t \eta = -\partial_x u - \partial_y v, \tag{1a}$$

$$\partial_t u = -\partial_x \eta + (f + \epsilon\nabla^2)v, \tag{1b}$$

$$\partial_t v = -\partial_y \eta - (f + \epsilon\nabla^2)u, \tag{1c}$$

where (u, v) are the two velocity components in the plane (x, y), η the interface elevation relative to the mean depth $H = 1$, f the Coriolis parameter and ϵ the odd viscosity parameter [67]. Time unit has been chosen such that phase speed is $\sqrt{gH} = 1$, with g the standard gravity. In the absence of odd viscous terms (when $\epsilon = 0$ above) it was realized that equatorial waves on Earth could be interpreted as topological modes of this flow when f varies with y and changes sign at the equator [43]. In what follows, we consider both f and ϵ positive and homogeneous in space. For geophysical fluids, ϵ is nothing but an arbitrarily small regularization parameter, in contrast to active matter systems described by a similar model and where ϵ can be tuned to large values. Indeed, this models occurs in various context beyond geophysical fluids [52,54,68] and appears as a paradigmatic two-dimensional model with three bands and spin-1 symmetry, by analogy

with the Dirac Hamiltonian that has two bands and spin-1/2 symmetry. We also discuss the latter in detail in Sec. VI.

A. The bulk picture

We briefly recall some known facts about the bulk problem, where $(x, y) \in \mathbb{R}^2$. We look for normal modes of the form $(\eta, u, v) = (\hat{\eta}, \hat{u}, \hat{v})e^{i(\omega t - k_x x - k_y y)}$ leading to the eigenvalue problem

$$\omega \begin{pmatrix} \hat{\eta} \\ \hat{u} \\ \hat{v} \end{pmatrix} = \begin{pmatrix} 0 & k_x & k_y \\ k_x & 0 & -i(f - \epsilon k^2) \\ k_y & i(f - \epsilon k^2) & 0 \end{pmatrix} \begin{pmatrix} \hat{\eta} \\ \hat{u} \\ \hat{v} \end{pmatrix}. \quad (2)$$

There are three bands: $\omega_\pm = \pm\sqrt{k^2 + (f - \epsilon k^2)^2}$ with $k^2 = k_x^2 + k_y^2$ and $\omega_0 = 0$. These band will be reminiscent in the edge picture, see below. In particular, the system is gapped for $f \neq 0$ and each band has a well-defined topological invariant: the Chern number. Respectively, $C_\pm = \pm 2$ and $C_0 = 0$ for $f > 0$ and $\epsilon > 0$. Each nonvanishing Chern number captures a twist in the corresponding eigenfunction $(\hat{\eta}_\pm, \hat{u}_\pm, \hat{v}_\pm)$ as (k_x, k_y) varies over $\mathbb{R}^2$. It is actually not well-defined for $\epsilon = 0$ and it was realized recently that odd-viscosity ensures that the bulk problem is properly regularized [52,53]. This is analogous to the regularization of Dirac Hamiltonian [29,64] (see also Sec. VI). The main issue that remains is the regularization of the edge picture.

B. The edge picture

In the edge picture, where $(x, y) \in \mathbb{R} \times \mathbb{R}^+$, we study three boundary conditions that are relevant for the topological aspects:

$$\text{DD:} \quad v(y = 0) = 0, \quad u(y = 0) = 0, \quad (3a)$$

$$\text{DM:} \quad v(y = 0) = 0, \quad (\partial_x u + \partial_y v)|_{y=0} = 0, \quad (3b)$$

$$\text{DS:} \quad v(y = 0) = 0, \quad (\partial_x u - \partial_y v)|_{y=0} = 0. \quad (3c)$$

In the following, we call (3a) Dirichlet-Dirichlet (DD), also called no-slip; (3b) is called Dirichlet-Membrane (DM), by noticing that from (1a), it implies $\partial_t \eta = 0$ at the boundary; (3c) is called Dirichlet-Stressfree (DS) since it imposes a vanishing force by the boundary on the fluid. We stress that each boundary condition consist of two constraints only. In particular, η is not always constrained. Moreover not all the constraints are allowed because the self-adjointness of the problem has to be preserved. For example, $u = 0$ and $\eta = 0$ at $y = 0$ is not an adequate boundary condition. See Appendix A for a general rule of the allowed boundary conditions.

The system is invariant under translation in the x direction so we look for normal modes of the form $(\eta, u, v) = (\hat{\eta}, \hat{u}, \hat{v})e^{i(\omega t - k_x x)}$. Inserting it into (1a) we realize that $\hat{\eta} = \omega^{-1}(k_x \hat{u} + i\partial_y \hat{v})$ can be eliminated when inserted into (1b) and (1c). We end up with a system of two ordinary differential equations of order two in y and with constant coefficients, depending on the parameters ω and k_x:

$$\left(\epsilon\partial_{yy} - \frac{k_x}{\omega}\partial_y + \left(f - \epsilon k_x^2\right)\right)\hat{v} = \frac{i}{\omega}\left(\omega^2 - k_x^2\right)\hat{u}, \quad (4)$$

$$\left(\epsilon\partial_{yy} + \frac{k_x}{\omega}\partial_y + \left(f - \epsilon k_x^2\right)\right)\hat{u} = -\frac{i}{\omega}(\partial_{yy} + \omega^2)\hat{v}. \quad (5)$$

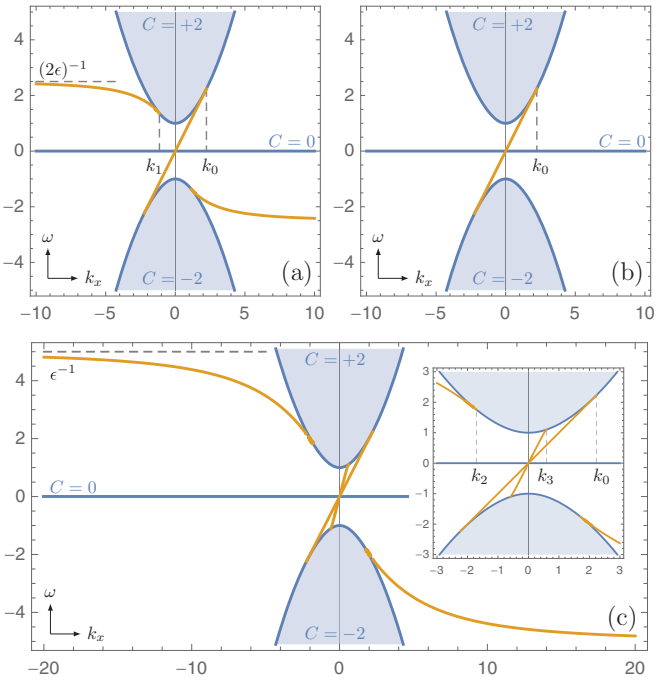

FIG. 2. Edge modes confined at the boundary $y = 0$ for $f = 1$, $\epsilon = 0.2$, and three different boundary conditions, according to (3): (a) DD, (b) DM, and (c) DS. In all cases, the Kelvin wave is present, with linear dispersion relation and $|k_x| < k_0$. For DM, this is the only mode. For DD (respectively, DS) one has an extra mode merging into the upper band at k_1 (respectively, k_2) and saturating at $\omega = 1/(2\epsilon)$ (respectively, ϵ). For DS, there is a third mode with almost linear dispersion relation $\omega \sim 2k_x$ and merging with the bulk at k_3. The blue curves delimits the region of the (projected) bulk bands.

This problem is solvable analytically. We look for solutions that are confined near the boundary, namely such that $(u, v) \to 0$ as $y \to \infty$. In contrast to bulk normal modes, such solutions appear in the gapped region of the (k_x, ω) plane, complementary to the (projected) bulk bands. We first solve the general problem for any value of k_x and ω in that region, then apply successively the different boundary conditions (DD, DM, and DS). The details are provided in Appendix B and the result is shown in Fig. 2.

We observe that the number of modes in each gap, which is supposed to be topological, depends on the choice of the boundary condition. In each gap, we respectively count 2, 1, and 3 modes for DD, DM, and DS. Moreover we observe the presence of edge modes leaving a bulk band and saturating at some constant frequency $\omega \propto \epsilon^{-1}$, showing that the edge problem is not compactified at $k_x \to \infty$, even if the bulk is. Moreover, the way to count these edge modes correctly is also puzzling, but the total number can anyway not coincide with the Chern number as it depends on the boundary condition. The bulk-edge correspondence seems anomalous.

III. ANOMALOUS BULK-EDGE CORRESPONDENCE

We define in this section a precise number of edge modes to quantify properly the bulk-edge correspondence anomaly reported in the previous section. This is an essential step to solve the paradox in the next section.

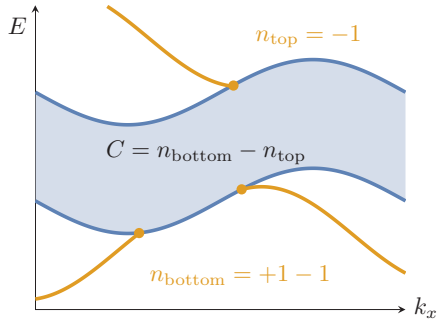

FIG. 3. The standard bulk-edge correspondence in its most general form. The number of edge modes (orange) below and above the bulk band (shaded blue) is defined by the crossing with its external lines (solid blue). The sign depends if the mode is disappearing or emerging in the bulk band, with a relative global sign for the top and the bottom.

A. Bulk-edge correspondence in condensed matter

Consider a conventional band of a Hamiltonian ruling a two-dimensional system, e.g., a tight-binding model, with Chern number C. In the edge picture (half-plane geometry with boundary at $y = 0$), the projection of this band may be connected to edge modes coming from the gap above and below, as illustrated in Fig. 3. As k_x is increasing, these modes can disappear into the band or emerge from it. For the bottom of the band, we *define* the number of edge modes n_{bottom} as the algebraic counting of the points where an edge state disappears $(+1)$ or emerges (-1). For the top of the band, we define similarly n_{top}, except that the signs are inverted [69]. This is equivalent to count the number of crossing of edge modes with the external lines of the bulk band, with a sign depending on the dispersion relation $\frac{\partial E}{\partial k_x}$ at the crossing. The bulk-edge correspondence is given by [10]

$$C = n_{\text{bottom}} - n_{\text{top}}. \tag{6}$$

Moreover if the problem satisfies a further assumption, quite common in condensed matter, this correspondence can be rewritten in a simpler form. Consider a system with N bands denoted by $i \in \{1, \ldots, N\}$, ordered by increasing energy and separated by spectral gaps, the corresponding topological numbers are C_i, n^i_{top}, and n^i_{bottom}. If we assume that both k_x and H are bounded (e.g., in a tight-binding model with a Brillouin zone), then necessarily $n^i_{\text{top}} = n^{i+1}_{\text{bottom}} := n^i$ for $1 \leqslant i \leqslant N - 1$ so that there is only one edge invariant n^i per gap i above the band i, that can be computed by the algebraic crossing with a horizontal line inside the gap (e.g., constant Fermi level). Moreover $n^1_{\text{bottom}} = 0$ and $n^N_{\text{top}} = 0$. In that case, the correspondence can be rewritten $n^i = -\sum_{j=1}^{i} C_i$, namely the number of edge modes in a gap is given by the sum of the Chern numbers of all band below it (up to a global sign depending of the orientation of the boundary) [10]. However, we claim that this relation is less general than (6), the latter being still satisfied when the previous assumption is not.

B. Anomaly in the continuous model

In the continuous model from Sec. II, neither k_x nor ω (analogue to E) are bounded so that the aforementioned assumption is not satisfied. We can however define a precise number of edge modes for each boundary condition, even for the modes that saturates asymptotically at a constant ω. This is summarized in Table I.

TABLE I. The number of edge modes around each band for different boundary conditions.

Boundary condition	DD	DM	DS
n^+_{bottom}	2	1	3
n^0_{top}	1	1	2
n^0_{bottom}	1	1	2
n^-_{top}	2	1	3

The middle band is never anomalous since $n^0_{\text{top}} = n^0_{\text{bottom}}$ regardless of the boundary condition, which is compatible with (6) and $C_0 = 0$. Moreover we notice that $n^0_{\text{top}} \neq n^+_{\text{bottom}}$ although it corresponds to the same gap between the middle and the upper band, but this is not a problem for the bulk-edge correspondence (6), since it focuses on a specific band rather than a gap. However the upper and lower band are anomalous: they are not bounded so the numbers n^+_{top} and n^-_{bottom} make no sense. If we naively set them to 0, then the bulk-edge correspondence is satisfied for DD boundary condition: $C_+ = n^+_{\text{bottom}} = 2$ and $C_- = -n^-_{\text{top}} = -2$, but we see immediately that the boundary conditions DM and DS are anomalous.

Nevertheless we claim that the bulk-edge correspondence (6) still makes sense, and the purpose of the next section is to provide a more general definition of the edge numbers, allowing for an explicit computation of n^+_{top} and n^-_{bottom} and so that (6) is restored for each band and any boundary condition.

IV. SCATTERING THEORY

In this section, we provide an alternative formalism to define and compute the number of edge modes above and below each band. As we shall see it reproduces the result from Table I independently, but it also allows for a definition of (generalized) edge modes at infinite ω, so that the bulk-edge correspondence (6) is recovered.

The formalism of scattering theory was developed in Ref. [19] to prove the bulk-edge correspondence for tight-binding models of condensed matter. We first review the general concepts involved and implement them explicitly in our case. The scattering matrix S encodes how bulk waves, that propagate *inside* the sample, are reflected at its edge [Fig. 4(a)]. The normal modes from Sec. II A are not solution to the boundary problem from Sec. II B, but a linear combination of an incoming state ψ_{in} and an outgoing state ψ_{out} can be. The scattering matrix S is then defined as the relative coefficient between these two states. See the precise definition below.

The interest of S resides in the application of Levinson's theorem [19]. At fixed k_x and for $\omega \to \omega_{\text{min}}(k_x)$, the bottom of the bulk band (when it exists), the argument of the scattering matrix is equal to the number of bound states below it [Fig. 4(b)]. In this context, they are precisely the edge modes that could appear below the bulk band. Then, as k_x increases, the argument of S stays the same until an edge mode disappears in (respectively, emerges from) the bulk band, in

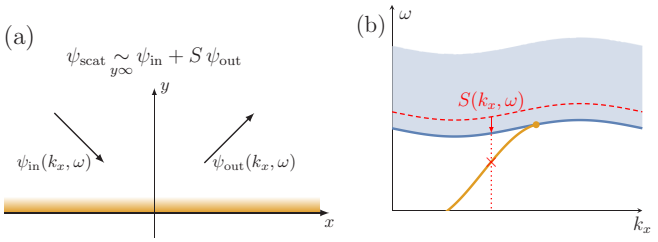

FIG. 4. The concept of scattering theory. (a) A linear combination, encoded by S, of incoming and outgoing bulk states is solution to the edge problem. (b) The scattering matrix [here a U(1) phase] is defined for k_x and ω in the projected bulk band. When approaching its extremity, the argument of S counts the number of bound states below: the edge modes in our case. As k_x varies, the relative argument of S counts the number of edge modes that have vanished (or emerged) in the band.

which case the argument changes by 2π (respectively, -2π). The number of edge modes between k_1 and k_2 is thus counted by [19]

$$n = \lim_{\varepsilon\to 0} \frac{1}{2\pi} \mathrm{Arg}[S(k_x, \omega_{\min}(k_x) + \varepsilon)]\Big|_{k_1}^{k_2}. \tag{7}$$

Note that a similar discussion is valid for the upper limit of the band (when it exists), up to a global sign. For usual condensed matter systems, we take $k_2 = k_1 + 2\pi$, namely a full loop over the reduced Brillouin zone, so that we get $n = n_{\rm bottom}$ from Sec. III A. In our case, we will take $k_1 \to -\infty$ and $k_2 \to \infty$.

A. The scattering matrix

To define S we recall some data from the bulk. For the rest of the discussion, we focus on the upper bulk band since the lower one can be studied in an analogous way. The normal mode associated to (2) and $\omega = \omega_+$ is $(\eta, u, v) = \hat{\psi} e^{i(\omega t - k_x x - k_y y)}$ with

$$\hat{\psi}(k_x, k_y) = \frac{1}{\sqrt{2}\,k} \begin{pmatrix} k^2/\omega_+(k) \\ k_x - ik_y(f - \epsilon k^2)/\omega_+(k) \\ k_y + ik_x(f - \epsilon k^2)/\omega_+(k) \end{pmatrix}. \tag{8}$$

This family is singular at $k = 0$ and $k \to \infty$ but each singularity can be removed up to a gauge transformation: $\hat{\psi}_{0/\infty} := \lambda_{0/\infty}\psi$ where $\lambda_0 = k^{-1}(k_x + is_f k_y)$ and $\lambda_\infty = k^{-1}(k_x - is_\epsilon k_y)$ are U(1) phases (s_f and s_ϵ are the respective sign of f and ϵ), see Ref. [53]. In the following, we shall consider $\hat{\psi}_0$ or $\hat{\psi}_\infty$ according to the region we are looking at.

In the edge picture, we fix $\omega > f$ and k_x in the projected bulk band and away from the singular points, and denote $k_y := \kappa$ to emphasize that it is not conserved. In the bulk, it is a fact that the equation $\omega_+(k_x, \kappa) = \omega$ always has at least two real solutions in κ, and possibly other solutions with nonvanishing imaginary part [19]. In our case, $\omega^2 = k_x^2 + \kappa^2 + (f - \epsilon(k_x^2 + \kappa^2))^2$ has four solutions in κ, that we denote by $\kappa_{\rm in/out} = \mp\sqrt{K_+}$ and $\tilde{\kappa}_\pm = \pm i\sqrt{-K_-}$, where

$$K_\pm = \frac{1}{2\epsilon^2}\big[-\big(1 - 2\epsilon\big(f - \epsilon k_x^2\big)\big) \pm \sqrt{1 - 4\epsilon f + 4\epsilon^2\omega^2}\big]. \tag{9}$$

Indeed for ω and k_x in the region of the upper bulk band, $K_+ \geqslant 0$ and $K_- \leqslant 0$ so that $\kappa_{\rm in/out} \in \mathbb{R}$ and $\tilde{\kappa}_\pm \in i\mathbb{R}$. Since $\frac{\partial\omega_+}{\partial\kappa} < 0$ for $\kappa = \kappa_{\rm in}$ then $\psi_{\rm in} := \hat{\psi}(k_x, \kappa_{\rm in}) e^{i(\omega_+ t - k_x x - \kappa_{\rm in} y)}$ is an incoming normal mode at frequency ω_+. Similarly $\kappa_{\rm out}$ describes an outgoing mode $\psi_{\rm out}$. The two other solutions describe modes that are exponentially increasing and decreasing away from the boundary $y = 0$. One of them is allowed and is a bound state, namely $\psi_{\rm b} := \hat{\psi}(k_x, \tilde{\kappa}_-) e^{i(\omega_+ t - k_x x)} e^{-|\tilde{\kappa}_-| y}$. This state is actually necessary to satisfy nontrivially the constraints of a boundary condition. The scattering state is defined by

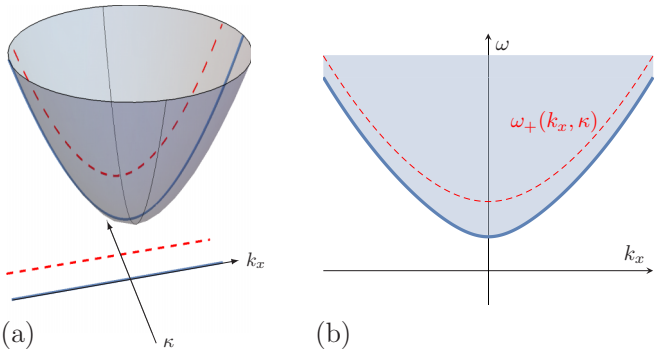

FIG. 5. (a) 3D Plot of the bulk band $\omega_+(k_x, \kappa)$. The red dashed curve is $\omega_+(k_x, \kappa)$ for fixed κ and the blue one is for $\kappa = 0$. (b) Projection of ω_+ in the edge picture. We shall look at the winding number of the scattering matrix as k_x varies along the dashed red curve, namely, for fixed κ, and then take the limit $\kappa \to 0$.

$$\psi_{\rm scat}(x, y, t) = \alpha\psi_{\rm in} + \beta\psi_{\rm out} + \gamma\psi_{\rm b} \tag{10}$$

with α, β, and γ are coefficients that depends on k_x and ω which are adjusted to satisfy the boundary condition at $y = 0$, so that $\psi_{\rm scat}$ is a solution of the edge problem as a superposition of bulk solutions. The scattering matrix is

$$S(k_x, \omega) := \frac{\beta}{\alpha}. \tag{11}$$

In our case, the eigenspace is of dimension 1, so that $S \in U(1)$ (the unitarity is ensured by a proper normalization of the scattering state [19]).

B. Bottom band scattering

We would like to look at the scattering matrix along the bottom of the band ω_+ instead of a fixed ω. In the edge picture the bulk band is projected: for fixed κ, $\omega_+(k_x, \kappa)$ describes a curve into the bulk band region that goes to the bottom of it when $\kappa \to 0$, see Fig. 5.

Thus we consider the scattering problem at fixed k_x and κ, the latter being small, and $\omega = \omega_+(k_x, \kappa)$. Then we look at the winding number as k_x varies, and eventually take the limit $\kappa \to 0$. We now set $\kappa_{\rm in} = -\kappa < 0$ and deduce from (9) and definitions of $\kappa_{\rm out}$ and $\tilde{\kappa}_\pm$ below it that $\kappa_{\rm out} = -\kappa_{\rm in} = \kappa$ and

$$\tilde{\kappa}_- = -i\sqrt{\kappa^2 + \frac{1}{\epsilon^2}\big(1 - 2\epsilon\big(f - \epsilon k_x^2\big)\big)}. \tag{12}$$

In particular, notice that $\lim \tilde{\kappa}_- \neq 0$ as $\kappa \to 0$. The scattering state becomes

$$\psi_{\rm scat}(y) = \alpha\hat{\psi}_0(k_x, -\kappa)e^{i\kappa y} + \beta\hat{\psi}_0(k_x, \kappa)e^{-i\kappa y} + \gamma\hat{\psi}_0(k_x, \tilde{\kappa}_-(k_x, \kappa))e^{-|\tilde{\kappa}_-(k_x,\kappa)|y}. \tag{13}$$

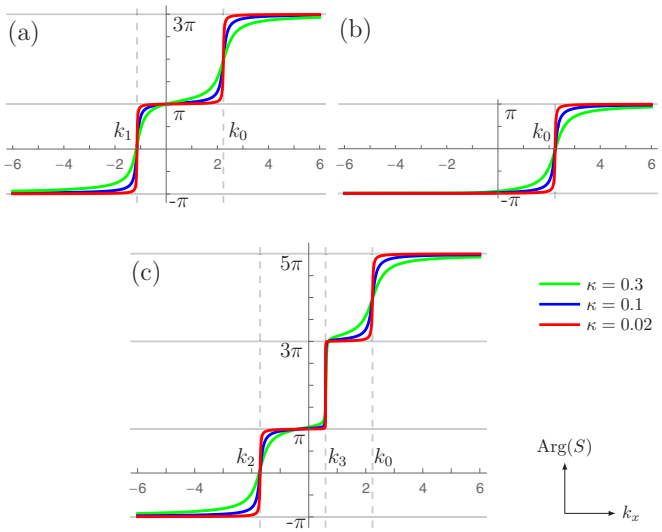

FIG. 6. Argument of S at the bottom of the band ω_+ for $f = 1$, $\epsilon = 0.2$, and $\kappa = 0.3,\ 0.1$, and 0.02 (respectively in green, blue, and red) for different boundary conditions. For DD (a), DM (b), and DS (c), the winding number of S is -2, -1, and -3, in agreement with n^+_{bottom} from Table I. The points $k_x = k_i$, where the jumps occur in the $\kappa \to 0$ limit, are the same than in Fig. 2 where the edge modes merge into the bulk band.

We dropped the x and t dependence that is trivial, and used $\hat{\psi}_0$ that is regular around $k_x, \kappa = 0$. Then we impose a boundary condition from (3) that will constraint two of the three parameters α, β, and γ, allowing a nonambiguous definition of $S(k_x, \kappa) = \beta/\alpha$. Note that this is not a coincidence: the number of conditions required at the boundary is deeply related to the number of solutions κ to $\omega_+(k_x, \kappa) = \omega$, which fixes the number of free parameters in the scattering states [19].

For each boundary condition in (3), we can define and compute $S \in \mathrm{U}(1)$ and look at its complex argument at the bottom of ω_+, namely, when k_x varies from $-\infty$ to $+\infty$ and $\kappa \to 0$. The scattering data is detailed in Appendix C and the argument of S is plotted in Fig. 6. We observe that the winding number of S is $w^+_{\text{bottom}} = 2,\ 1$, and 3, respectively, for DD, DM, and DS, in agreement with n^+_{bottom} from Table I. Moreover, as $\kappa \to 0$, the jump of Arg(S) occurs precisely at the points $k_x = k_i$ ($i = 0, \ldots, 3$) where the edge modes merge into the bulk band, compare with Fig. 2.

C. Infinite top band scattering

As we have seen the scattering formalism provides an alternative way to compute the number of (standard) edge modes below the band, that is consistent with the method from Sec. III. However, it is more general than the latter because it allows to count the number of edge modes at the top of the band, even if the upper band is not bounded from above. Indeed, we simply compute the scattering matrix as before, but instead we take $\kappa \to \infty$, which corresponds to the (infinite) edge of the upper band. Moreover, in that case, we are near the $k \to \infty$ point that may be singular, so we compute the scattering data with $\hat{\psi}_\infty$ that has no singularity there, instead of $\hat{\psi}_0$. This is done in Appendix C and the argument of S is plotted in Fig. 7.

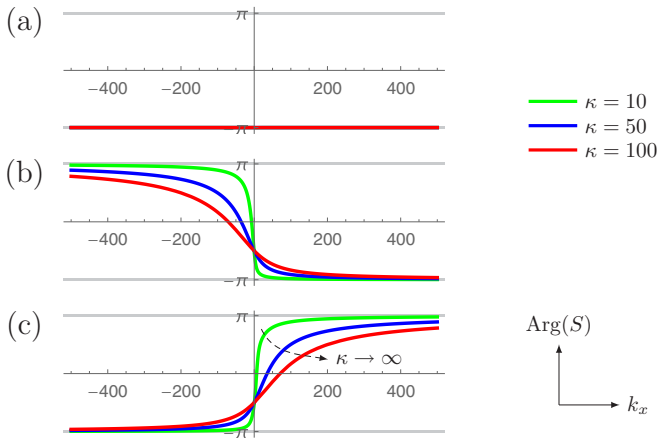

FIG. 7. Argument of S at the (infinite) top of the band ω_+ for $f = 1$, $\epsilon = 0.2$, and $\kappa = 10$, 50, and 100 (respectively, in green, blue, and red) with different boundary conditions. For DD (a) the three curved are superposed to the constant value π, so that S does not wind. For DM (b) and DS (c) one has a nonvanishing winding number: respectively, -1 and 1. Note that the red curve is the closest to the $\kappa \to \infty$ limit, so that this winding is delocalized in k_x, rather than converging to a localized jump, in contrast to the scattering at the bottom of the band (Fig. 6).

We observe that S has a well-defined winding number for DD, DM, and DS as we explore the upper limit of the band: respectively, 0, -1, and 1. Moreover we stress that in this limit the argument of S is *not* converging to a localized jump but rather completely delocalized in k_x, so that one has to explore the whole parameter $k_x \in \mathbb{R}$ in order to compute it. Finally we call this winding number n^+_∞, which we interpret as the number of edge modes at the (infinite) top of the band ω_+. If we compare it with the edge number at the bottom of the band, we conclude that the bulk-edge correspondence (6) is not anomalous anymore, namely, the difference between the two numbers always gives the Chern number of the upper band (see Table II).

V. SOME PHYSICAL CONSEQUENCES

The scattering matrix detects the presence of generalized edge modes at infinite frequency that we dub *ghost modes*. *A posteriori*, we can actually see a footprint of these modes at finite frequency from various perspectives.

A. Channel geometry

A striking manifestation of shallow water ghost modes is found when considering a channel (or ribbon) geometry of

TABLE II. The number of (generalized) edge modes for the upper band. The bulk-edge correspondence (6) is properly satisfied regardless of the boundary condition if we identify $n^+_\infty = n^+_{\text{top}}$.

Boundary condition	DD	DM	DS
n^+_∞	0	-1	1
n^+_{bottom}	2	1	3
C_+	2	2	2

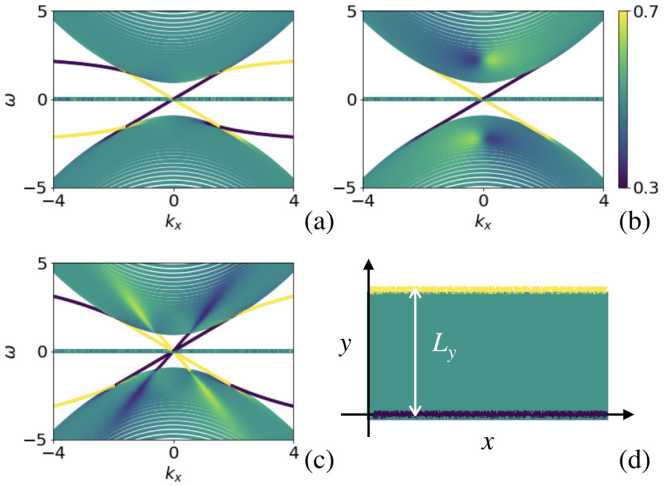

FIG. 8. Shallow water spectrum with condition DD (a), DM (b), and DS (c) for a channel geometry of size L_y (d). The color bar indicates the localization of each state along the transverse direction. On top of edge modes, one also observes quasilocalized states in the bulk bands, in agreement with the existence and position of ghost modes from the semi-infinite configuration.

finite size L_y. We compute numerically such a spectrum using DEDALUS code [70,71] for each boundary condition discussed above, see Fig. 8. The same condition is used at both edge. In the three cases, we recover both bulk bands and edge modes, as computed analytically in the semi-infinite case. However, we also notice that some of the bulk modes are actually quasilocalized at one of the channel edges for DM and DS. We check that this quasilocalization vanishes as $L_y \to \infty$ for a given k_x and ω. Thus, although such effect appears at both edges, it seems impossible to see it on each one separately, in contrast to standard edge modes. Hence this quasilocalization may be interpreted as a resonant state between the two edges.

We interpret such a quasilocalisation effect within the bulk band as a manifestation of the ghost modes computed in the semi-infinite case: for DD, no ghost mode is found and no quasilocalized state is obtained here; for DM, one ghost mode is obtained at infinite ω and negative k_x [see Fig. 7(b)], consistently with a quasilocalized mode that originates from the bulk itself (this mode becomes more and more delocalized as ω increases towards negative k_x); for (DS), one ghost mode is found at infinite ω and positive k_x [see Fig. 7(c)], consistently with the quasilocalized bulk mode that seems to originate from one of the three edge modes in the gap. Moreover, in (b) and (c), there is a peak of maximal quasilocalization for a given ω in the bulk wave band. Such a peak becomes less intense and more spread as ω increases, and has a well-defined dispersion relation which slope's sign matches with n_∞^+. These observations suggest that measuring the spatial structure of wave-band eigenmodes in a finite geometry could be a way to probe at finite ω the presence of ghost modes in the shallow water system.

B. Local density of states

In a semi-infinite geometry, it is possible to observe a similar effect in the bulk spectrum by studying the local density of states $\rho(y, \omega)$. It can be computed analytically thanks to the explicit expression of ψ_{scat}, see Appendix D. It reads

$$\rho(y, \omega) = \rho_0(\omega) + \int_{-k_{\max}}^{k_{\max}} dk_x \, \mathcal{R}(y, k_x, \omega), \tag{14}$$

where ρ_0 is the "free" part in absence of boundary and $k_{\max}(\omega)$ is the maximal value of k_x in the bulk band for a given ω. The quantity $\mathcal{R}(y, k_x, \omega)$ represents the excess of local density of states due to the presence of a boundary. It is plotted for $y = 0$ in Fig. 9 and each boundary condition.

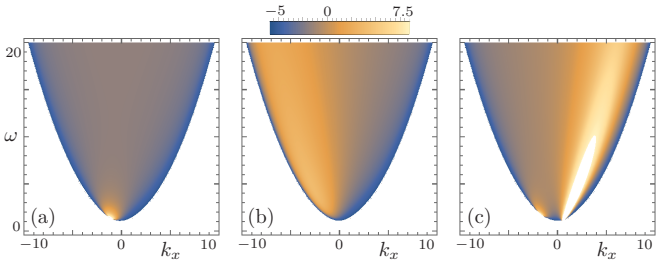

FIG. 9. Excess of local density of states $\mathcal{R}(y = 0, k_x, \omega)$ at the boundary for (a) DD, (b) DM, and (c) DS boundary conditions. The diffuse peaks appearing in the two latter cases is reminiscent of ghost modes.

For boundary condition DD, $\mathcal{R}$ is homogeneous and close to zero almost everywhere, except at the limit of the band where it diverges (slowly) as $k_x \to k_{\max}$. Moreover, it also shows a peak at the bottom of the spectrum, which is reminiscent of some proper edge modes merging with the bulk band. $\mathcal{R}$ shares similar features for DM and DS but with an extra diffuse peak, respectively, on the left and the right of the spectrum, in agreement with the previous section. However, even though Figs. 8 and 9 bear striking similarities, the interpretation is different: a peak for $\mathcal{R}$ does not necessarily imply the decay of the corresponding state as $y \to \infty$. Nevertheless, we interpret such a peak as a manifestation at finite ω of the existence of a ghost mode near $k_x \to \pm\infty$. In particular, the value of n_∞ can be read of the "dispersion relation" of the diffuse peak.

Moreover, the local density of states is closely related to the scattering matrix S, emphasizing its physical relevance. Indeed, the expression for $\mathcal{R}$ involves the quantity $\mathcal{S}(k_x, \omega) = \langle \hat{\psi}_{\text{in}}, S\hat{\psi}_{\text{out}} \rangle$, see (D6). This dressed S matrix also matches with the one of [72]. Remarkably, $\mathcal{S}$ is gauge invariant, in contrast to S that depends on the choice of ψ. Moreover, it also counts the number of ghost modes:

$$\int_{-k_{\text{m}}}^{k_{\text{m}}} \mathcal{S}^* \frac{\partial S}{\partial k_x} dk_x = 2\pi i n_\infty^+ \tag{15}$$

for any ω finite but sufficiently large, similarly to Fig. 7. Thus the presence of ghost modes ($n_\infty^+ \neq 0$) has a concrete physical manifestation on the local density of states at finite ω via $\mathcal{R}$.

C. Inertial-like edge modes at infinity

Finally, to connect ghost modes with previous works from the fluid dynamics literature, we study perturbatively the asymptotic regions of the gap in the limit of large wave

number $|k_x|$. Let us consider $\epsilon > 0$, $f > 0$ and let us assume $\omega = \alpha|k_x|^\beta$ for some $1 < \beta < 2$ and $\alpha > 0$ (i.e., below the band ω_+ when $k_x \to \pm\infty$). At the leading order in k_x, the solutions localized near the edge are of the form [see (B14) and (B19)]

$$v(y) \sim V_3 e^{s_+ y} + V_4 e^{s_- y}, \tag{16}$$

$$u(y) \sim -i(V_3 e^{s_+ y} - V_4 e^{s_- y}), \tag{17}$$

where $s_\pm = -|k_x|(1 \pm \frac{\alpha}{2\epsilon}|k_x|^{\beta-2})$.

These solutions are superpositions of inertial-like waves, defined as waves with polarization relation $(\eta, u, v) = (0, 1, \pm i)$. In the absence of odd viscosity, these waves are constant frequency modes $\omega = \pm f$, hence their name inertial. Because the odd viscous terms added into the problem have the structure of the Coriolis force (but depending on the wave number), it is not surprising that we recover such states at large wave numbers.

The possible existence of a solution is discussed by applying the different boundary conditions. In the three cases considered above, the impermeability constraint $v(0) = 0$ leads to $V_4 = -V_3$. Thus, for DD (3a), the second condition $u(0) = 0$ leads to $V_3 = 0$ so that there is no asymptotic mode, in agreement with $n_\infty^+ = 0$. However, for DM (3b), we get from (B30) the condition $2k_x = -(\alpha/\epsilon)|k_x|^{\beta-1}$ to have $V_3 \neq 0$. For $k_x \to -\infty$, there is a solution when $\beta \to 2$ and $\alpha = 2\epsilon$. Instead, for $k_x \to +\infty$, there is no solution. This indicates the presence of an edge mode in the asymptotic upper-left region of the spectrum, whereas upper-right is empty. That is consistent with Fig. 7(b) where the jump of the argument seems to be "pushed" to $k_x \to -\infty$ as $\kappa \to +\infty$. Thus the scattering matrix counts the mismatch in the number of modes between $k_x = -\infty$ and $+\infty$. In this picture, it seems that one mode has merged from the right to the "top" of the band, in agreement with $n_\infty^+ = -1$. Conversely, for DS the asymptotic expansion indicates the presence of a mode in the upper-right region, in agreement with Fig. 7(c) and $n_\infty^+ = +1$.

Interestingly, in the context geophysical fluid dynamics, an interpretation of the dispersion relation in shallow-water models with different boundary conditions was proposed by Iga [55], also by considering different asymptotic regimes in (k_x, ω) diagram. In these regimes, the initial problem is simplified and more tractable. Using an argument based on the conservation of the eigenfunction's zeros when k_x is varied, Iga predicted the global shape of the spectra [55], and generalized this method to other geophysical flow models [57]. This method gives robust information on the spectrum, such as the existence of modes that transit from one band to another when k_x is varied (spectral flow), under fairly general assumptions (channel or cylinder geometry, parameters enforcing the existence of discrete spectrum, etc.). Here we have provided a complementary point of view using topology, where, again, asymptotic regions of the (k_x, ω) diagram must be taken into account to understand to the global shape of the spectrum.

VI. DIRAC HAMILTONIAN

The choice of the shallow-water model was made here to illustrate the consequences on coastal waves in classical fluids, but our analysis of the bulk-edge correspondence applies to any two dimensional continuous model, as long as the bulk problem is properly compactified.

Postponing a general rigorous theorem to future work, we illustrate the power of our approach by applying the scattering formalism to the celebrated (massive) Dirac Hamiltonian, regularized by a ϵk^2 mass term

$$H = \begin{pmatrix} m + \epsilon(\partial_x^2 + \partial_y^2) & i\partial_x + \partial_y \\ i\partial_x - \partial_y & -m - \epsilon(\partial_x^2 + \partial_y^2) \end{pmatrix}. \tag{18}$$

Such an Hamiltonian could describe for instance a two-dimensional ^{3}He-A superfluid phase, where the mass term m would correspond to the chemical potential [29].

When the mass m is fixed, the presence of a regularization term ϵk^2 makes possible the introduction of well-defined Chern numbers of value

$$C_\pm = \pm\frac{\mathrm{sign}(m) + \mathrm{sign}(\epsilon)}{2} \tag{19}$$

for the two eigenstates $\psi_\pm(k_x, k_y)$ of the bulk Hamiltonian

$$H_{\mathrm{bulk}} = \begin{pmatrix} m - \epsilon k^2 & k_x - ik_y \\ k_x + ik_y & -m + \epsilon k^2 \end{pmatrix} \tag{20}$$

with $k^2 = k_x^2 + k_y^2$, that is derived from (18) by using a Fourier basis $e^{-i(k_x x + k_y y)}$ (see Appendix E and Ref. [64]).

Let us then set m and ϵ so that $C_+ = 1$ and address the question of the boundary modes. For that purpose, we consider two different boundary conditions for $\psi := (\phi_1, \phi_2)^T$ at $y = 0$ that satisfy hermiticity (see Appendix A)

$$\text{A:} \quad \phi_1|_{y=0} = 0, \quad \phi_2|_{y=0} = 0, \tag{21a}$$

$$\text{B:} \quad \phi_1|_{y=0} = 0, \quad \partial_y\phi_2|_{y=0} = -i\partial_x\phi_2|_{y=0}. \tag{21b}$$

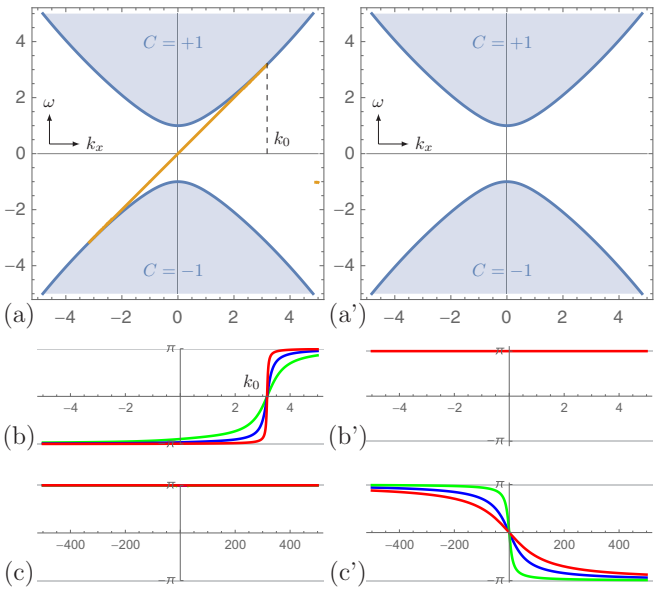

FIG. 10. Dirac Hamiltonian with $m = 1$ and $\epsilon = 0.1$ (a) Edge spectrum with boundary condition A (21a) (b) Arg(S) at the bottom of the upper band, for $\kappa = 0.3$, 0.1, and 0.02 (respectively in green, blue, and red) (c) Arg(S) at the "top" of the upper band, for $\kappa =$ 10, 50, and 100 (respectively in green, blue, and red). (a′), (b′) and (c′) are the same plots for condition B (21b).

The energy spectra for the boundary modes allowed by these two boundary conditions are derived in Appendix E and displayed in Fig. 10 for $m = 1$ and $\epsilon = 0.1$.

Boundary conditions A yield the naively expected result from the values of the Chern numbers $C_\pm = \pm 1$, namely one chiral boundary mode that spans the bulk gap and propagates to the right (positive group velocity). The merging of this chiral mode into the bulk bands at $k_0 \approx \pm 3$ is well captured by the scattering theory introduced above and applied for the Dirac case in Appendix E. Figure 10 shows that this winding is indeed $+1$ for the top band, with a jump in phase that exactly occurs at $k = k_0$. It is also checked that no other evanescent state enters the band at $\omega \sim \infty$ ($n^+_\infty = 0$), so that the winding number equals the Chern number and captures the number of modes gained by the bulk band.

In contrast, the boundary condition B does not allow boundary mode at finite energy and k. Accordingly, the winding number is zero meaning that there is no evanescent mode entering the bulk bands. However, the winding $n^+_\infty = -1$ indicates the entrance of an *ghost* boundary mode from the "top" of the band of positive energy, in agreement with the bulk-boundary correspondence, and the value of the Chern number.

VII. DISCUSSION

To conclude, the apparent paradox of a mismatch in the bulk-edge correspondence for a continuous model with a sharp boundary is solved by the presence of "ghost" edge modes at infinity, that can be detected through the scattering formalism. Thus, in continuous media, the bulk-edge correspondence is always satisfied, independently from the boundary condition. This new paradigm can indeed be applied to any continuous model. Moreover, it has various consequences and paves the way for new directions of investigation that we discuss now.

a. Contrary to a common belief, chiral is not topological. A usual way to define the edge number is to count the algebraic crossing number $n_{\text{cross}}(\omega)$ of the edge modes dispersion relation with a horizontal line $\omega = C^{te}$ in the gapped region (analogue to the Fermi energy in condensed matter). For continuous models, this number is still well defined but not relevant for the bulk-edge correspondence: it actually depends on the choice of boundary condition. Furthermore, even for a fixed boundary condition, this number can jump while varying continuously a parameter of the Hamiltonian without closing the gap in the bulk, or while varying ω with all parameters fixed. See Fig. 11.

This is rooted in the fact that an edge mode in continuous media is *not* necessarily connected to bulk bands at both of its extremities. It may leave a band without connecting another one and escape in the infinite gapped region. This is reminiscent to the fact that the edge problem may not be compactified, even if the bulk problem is. Importantly, the chirality of these *open* edge modes, namely the sign of their group velocity, can be tuned continuously from positive to negative. Worse, it is ill-defined when the dispersion relation reaches a constant value asymptotically.

Consequently, $n_{\text{cross}}(\omega)$ is in general not sufficient to conclude about the value of the bulk topological invariant. This paper shows that the correct edge number that matches in the bulk-edge correspondence is $n_{\text{top/bottom}} \neq n_{\text{cross}}(\omega)$. As discussed in Sec. III A these quantities are the same only if k_x and H are bounded, which is not always true in continuous models.

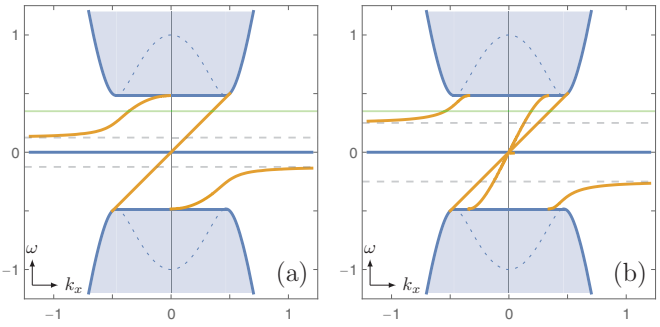

FIG. 11. Edge modes for $f = 1$ and *large* $\epsilon = 4$, with two different boundary conditions according to (3): (a) DD and (b) DS. The number n_{cross}, counting the crossing between the edge modes and the green horizontal line is respectively 2 and 3, but would be 1 and 2 in the case where ϵ is small [compare with Figs. 2(a) and 2(c)]. Moreover, if we move the green line below some threshold $\propto \epsilon^{-1}$ (horizontal dashed line), or if we decrease ϵ continuously, then n_{cross} is also lowered by 1.

However we believe than $n_{\text{cross}}(\omega)$ could still be of interest because the chiral edge modes detected that way are still robust against defects on the boundary, as discussed in Ref. [52]. In principle we expect these modes to be also stable under a disordered potential so that, although not topological, $n_{\text{cross}}(\omega)$ could still be protected but in a weaker sense that has to be investigated. We postpone the study of it to future work.

b. Coastal Kelvin are topologically protected in a weaker sense than equatorial Kelvin waves. Coastal Kelvin waves are unidirectional edge states trapped along a boundary with impermeability condition ($v = 0$ along the coast $y = 0$), and with a trapping length scale given by then Rossby radius of deformation $L_d = c/f$ [73], with c the phase speed of such waves. In Fig. 2 of the shallow-water model, they correspond to the edge mode with linear dispersion relation $\omega = ck_x$ with $c = 1$ and $|k_x| < k_0$. We notice that this mode is always present in the spectrum, while the other edge modes depend on the boundary condition. We conjecture this to be true whenever the boundary condition includes the impermeability constraint. Moreover all additional edge modes have a trapping length scale that tends to zero as $\epsilon \to 0$, contrary to the coastal Kelvin wave that coincides in that limit with its analog in absence of odd-viscosity ($k_0 \to \infty$). Finally it is robust to the continuous parameter deformation discussed above, and it is actually the only mode that is properly counted by spectral crossing $n_{\text{cross}}(\omega)$. The coastal Kelvin wave seems therefore more robust than other edge modes in presence of a sharp boundary.

However, in the case without odd-viscosity, coastal Kelvin waves can be removed from the spectrum just by relaxing the impermeability constraint [55], and we suspect the same to occur here, so that this mode is not topological in the strongest sense. This contrasts with unidirectional waves that are trapped along the equator of rotating atmospheres and

oceans, and called equatorial Kelvin (and Yanai) waves by analogy. There the equator is an interface where f changes sign. In contrast to a boundary, there is a canonical gluing condition for the interface, for which equatorial Kelvin wave is topological [43,53]. This is due to the bulk-interface correspondence that does not suffer from any anomaly. This correspondence is a manifestation of Atiyah-Singer index theorem, that was noted in other physical problems and then generalized to a wider class of models [35,64,65,74,75]. In the presence of a sharp boundary, as in this paper, the existence of an index theorem remains an open question.

c. Towards a detection of ghost edge modes? Finally, the number of ghost edge modes at infinite frequency n_+^∞ is not an abstract mathematical quantity. It has physical consequences, for example on the spectrum of a channel geometry or on the local density of states, as we have seen in Sec. V. Such effects could in principle be detected at finite frequency. Notice that there is a longstanding literature relating the scattering matrix with the density of states [72,76–78]. However, it mainly concerns problems with impurities instead of a hard wall that we consider here. There seems to be a connection between the two approaches, but the interpretation of a boundary condition in terms of a defect potential is not straightforward. Nevertheless, we expect that physical manifestations, such as Friedel oscillations, known to occur in the presence of defects will also be found in the presence of a wall, and will naturally be influenced by ghost modes through the scattering matrix $\mathcal{S}$. This is a promising but intricate issue that we postpone for future works.

Furthermore, in the shallow-water model for equatorial waves, odd viscosity was considered only as a rather small regularizing parameter. But odd-viscous terms must actually be taken into account to properly describe active matter fluids systems where microscopic time reversibility is broken [52,68]. Furthermore, the optical analog of the odd-viscosity is provided by a nonlocal gyroelectric effect that couples the two in-plane electric field components of the transverse magnetic modes [54]. These two examples could constitute versatile platforms for possible future spectral measures leading to the detection of ghost edge modes.

ACKNOWLEDGMENTS

C.T. is grateful to Gian Michele Graf and Hansueli Jud for many insightful discussions. P.D. and A.V. were partly funded by ANR-18-CE30-0002-01 and IDEX ToRe during this work.

APPENDIX A: ALLOWED BOUNDARY CONDITIONS

The allowed boundary conditions are constrained by looking at the self-adjointness of the problem. Rewriting (1) as $i\partial_t\psi = H\psi$ with $\psi = (\eta, u, v)$ we impose the condition $\langle\phi, H\psi\rangle = \langle H\phi, \psi\rangle$, for any $\phi, \psi \in L^2(\mathbb{R}\times\mathbb{R}^+)$. After a few integration by parts we end up with

$$i\int_{\mathbb{R}} dx(v_1^*(\eta_2+\epsilon\partial_y u_2)+(\eta_1^*+\epsilon\partial_y u_1^*)v_2 \\ -\epsilon((\partial_y v_1^*)u_2+u_1^*\partial_y v_2))|_{y=0}=0, \tag{A1}$$

which restricts the possible boundary conditions at $y=0$. We deduce that in general, only two constraints are required on (η, u, v). In particular, (3a)–(3c) are solution to (A1), but there exists many other possibilities for the shallow-water model.

Similarly, the Hermitian boundary conditions at $y=0$ for the regularized Dirac model (18) have to satisfy

$$\int_{\mathbb{R}} dx(-\phi_1^*\chi_2+\phi_2^*\chi_1-\epsilon(\phi_1^*\partial_y\chi_1-\chi_1\partial_y\phi_1^* \\ -\phi_2^*\partial_y\chi_2+\chi_2\partial_y\phi_2^*))|_{y=0}=0\,. \tag{A2}$$

This is the case for the two boundary conditions (21a) and (21b) discussed in the main text.

APPENDIX B: SOLVING THE EDGE PROBLEM

In this Appendix, we solve the system of ODE (4) and (5) in u and v (we dropped the hat to simplify the notations). In the gapped region of the (k_x,ω)-parameter plane, we look for solutions that vanish as $y\to\infty$. First we compute all such modes that could exist in general, and then specify each boundary condition and see the compatible solutions that persist. Moreover, in the following, we assume $f>0$, $\epsilon>0$ and $f\epsilon<1/4$. For the general problem, we proceed by disjunction. First note that $u\equiv 0$ leads to $v\equiv 0$, so this case is trivial.

a. Case 1: $v\equiv 0$. From (4), we infer $\omega^2=k_x^2$ that has two branches, $\omega=\pm k_x$. Since $v\equiv 0$ the solution to (5) is of the form

$$u(y)=Ae^{q_+ y}+Be^{q_- y}, \tag{B1}$$

where

$$q_\pm=-\frac{1}{2\epsilon}\left(\frac{k_x}{\omega}\pm\sqrt{1+4\epsilon\left(\epsilon k_x^2-f\right)}\right), \tag{B2}$$

that is always well defined as long as $f\epsilon\leqslant 1/4$. Notice that $q_\pm$, A and B depend on k_x and ω. For u to vanish at $y\to\infty$ we have either $q_\pm<0$ or $A/B=0$.

Case 1.a: $\omega=k_x$. One has $q_+<0$ for all k_x and $q_-<0$ only for $|k_x|<k_0:=\sqrt{f/\epsilon}$, so that

$$u(y)=\begin{cases}Ae^{q_+ y}+Be^{q_- y}, & |k_x|<k_0,\\ Ae^{q_+ y}, & |k_x|\geqslant k_0.\end{cases} \tag{B3}$$

Case 1.b: $\omega=-k_x$. One has $q_->0$ for all k_x and $q_+<0$ only for $|k_x|>k_0$, so that

$$u(y)=\begin{cases}0 & |k_x|\leqslant k_0,\\ Ae^{q_+ y}, & |k_x|>k_0.\end{cases} \tag{B4}$$

b. Case 2: $v\neq 0$ and $\omega^2=k_x^2$. We first solve (4) that is homogeneous for v. The solution is of the form

$$v(y)=Ae^{r_+ y}+Be^{r_- y} \tag{B5}$$

with

$$r_\pm=\frac{1}{2\epsilon}\left(\frac{k_x}{\omega}\pm\sqrt{1+4\epsilon\left(\epsilon k_x^2-f\right)}\right). \tag{B6}$$

The solution of (5) is a superposition of a homogeneous part, already given in the previous section, and a particular solution depending on the solution for v. Namely,

$$u(y)=Ce^{q_+ y}+De^{q_- y}+\alpha_+Ae^{r_+ y}+\alpha_-Be^{r_- y} \tag{B7}$$

with $q_\pm$ given in (B2) and

$$\alpha_\pm = -\frac{i}{\omega}(r_\pm^2+\omega^2)\left(\epsilon r_\pm^2 + \frac{k_x}{\omega}r_\pm + f - \epsilon k_x^2\right)^{-1}. \quad \text{(B8)}$$

Case 2.a: $\omega = k_x$. One has $r_+ \geqslant 0$ for all k_x and $r_- \geqslant 0$ for $|k_x| \leqslant k_0$ so that

$$v(y) = \begin{cases} 0 & |k_x| \leqslant k_0, \\ Be^{r_- y}, & |k_x| > k_0. \end{cases} \quad \text{(B9)}$$

Note that for $|k_x| \leqslant k_0$ we are back to Case 1, so we have to omit this region here to avoid double counting. Consequently,

$$u(y) = Ce^{q_+ y} + \alpha_- Be^{r_- y}, \quad |k_x| > k_0. \quad \text{(B10)}$$

Case 2.b: $\omega = -k_x$. One has $r_- < 0$ for all k_x and $r_+ < 0$ for $|k_x| < k_0$, so that

$$v(y) = \begin{cases} Ae^{r_+ y} + Be^{r_- y} & |k_x| \leqslant k_0, \\ Be^{r_- y}, & |k_x| > k_0, \end{cases} \quad \text{(B11)}$$

and

$$u(y) = \begin{cases} \alpha_+ Ae^{r_+ y} + \alpha_- Be^{r_- y} & |k_x| \leqslant k_0, \\ Ce^{q_+ y} + \alpha_- Be^{r_- y}, & |k_x| > k_0. \end{cases} \quad \text{(B12)}$$

c. Case 3: $v \neq 0$ *and* $\omega^2 \neq k_x^2$. In that case, u is entirely fixed by v through equation (4), and one can moreover combine (4) and (5) to get a fourth order homogeneous equation for v:

$$\left(\epsilon^2\partial_y^{(4)} + \left(2\epsilon\left(f-\epsilon k_x^2\right)-1\right)\partial_y^{(2)} + \left(f-\epsilon k_x^2\right)^2 - \left(\omega^2 - k_x^2\right)\right)v = 0. \quad \text{(B13)}$$

The corresponding algebraic equation always admits real solutions as long as $f\epsilon \leqslant 1/4$, given by $s^2 = S_\pm$ with

$$S_\pm = \frac{1}{2\epsilon^2}\left(1 + 2\epsilon\left(\epsilon k_x^2 - f\right) \pm \sqrt{1 + 4\epsilon(\epsilon\omega^2 - f)}\right). \quad \text{(B14)}$$

In the gapped region, one has

$$k_x^2 - \omega^2 + \left(f - \epsilon k_x^2\right)^2 > 0 \quad \text{(B15)}$$

leading to four real solutions to (B13)

$$s_1 = \sqrt{S_+}, \quad s_2 = \sqrt{S_-}, \quad s_3 = -\sqrt{S_+}, \quad s_4 = -\sqrt{S_-}. \quad \text{(B16)}$$

Notice that by construction $s_{1/2} > 0$ and $s_{3/4} < 0$ regardless of k_x, ω, or f. Consequently,

$$v(y) = V_3 e^{s_3 y} + V_4 e^{s_4 y} \quad \text{(B17)}$$

and by (4)

$$u(y) = \lambda_3 V_3 e^{s_3 y} + \lambda_4 V_4 e^{s_4 y}, \quad \text{(B18)}$$

where

$$\lambda_i = \frac{\omega}{i\left(\omega^2 - k_x^2\right)}\left(\epsilon s_i^2 - \frac{k_x}{\omega}s_i + f - \epsilon k_x^2\right). \quad \text{(B19)}$$

1. Edge modes

Now we specify a boundary condition from (3) and look at the modes from the previous section that are compatible with it.

a. Dirichlet/Dirichlet (DD). Here we impose (3a), namely, $u = v = 0$ at $y = 0$. In case 1, we infer immediately

$$u(y) = \begin{cases} A(e^{q_+ y} - e^{q_- y}), & |k_x| < k_0, \quad \text{and} \quad \omega = k_x \\ 0 & \text{otherwise.} \end{cases} \quad \text{(B20)}$$

and $v \equiv 0$. One has one mode (i.e., one free parameter A) living in a compact region [see Fig. 2(a)]. In case 2, the solutions are trivial for $\omega = k_x$, and $\omega = -k_x$ for $|k_x| > k_0$. The last possibility is

$$v(y) = A(e^{r_+ y} - e^{r_- y}), \quad |k_x| \leqslant k_0, \quad \text{(B21)}$$

but only if $u(y) = A(\alpha_+ e^{r_+ y} - \alpha_- e^{r_- y})$ vanishes at $y = 0$, which implies that $\alpha_+(k_x, -k_x) - \alpha_-(k_x, -k_x) = 0$. This generically occurs only for a finite number of k_x points, that are actually part of the edge modes from case 3. Apart from that there is no mode in that case. In case 3, the region of compatibility with the boundary conditions is given by

$$0 = \det\begin{pmatrix} 1 & 1 \\ \lambda_3(k_x,\omega) & \lambda_4(k_x,\omega) \end{pmatrix} = \lambda_4(k_x,\omega) - \lambda_3(k_x,\omega) \quad \text{(B22)}$$

for (k_x, ω) in the gapped region but away from the branches $k_x^2 = \omega^2$ that are forbidden by assumption. The latter constraint leads to

$$\epsilon(s_3(k_x,\omega) + s_4(k_x,\omega)) - \frac{k_x}{\omega} = 0 \quad \text{(B23)}$$

that is plotted in Fig. 2(a). We have one mode in each gap that stops in a bulk band at $k_x = k_1$ with

$$k_1 := \pm k_0 \sqrt{1 - \frac{3}{4f\epsilon}\left(1 - \sqrt{1 - \frac{16}{9}f\epsilon}\right)} \quad \text{(B24)}$$

on one side and saturates at $\pm\frac{1}{2\epsilon}$ as $k_x \to \pm\infty$. Along this curve, the kernel of the matrix appearing in (B22) is generated by $(1, -1)$, so that (B17) is a solution for $V_4 = -V_3$, namely,

$$v(y) = V_3(e^{s_3 y} - e^{s_4 y}), \quad u(y) = \lambda_3 V_3(e^{s_3 y} - e^{s_4 y}). \quad \text{(B25)}$$

Thus we have one edge mode in that case.

b. Dirichlet/membrane (DM). Here we impose (3b), namely $v = 0$ and $\partial_x u + \partial_y v = 0$ at $y = 0$. For the normal modes the latter condition can be rewritten $-ik_x u + \partial_y v = 0$. In Case 1 where $v \equiv 0$ it is equivalent to $u = 0$ at the boundary, so this is similar to the Dirichlet/Dirichlet problem from the previous section. Hence we have one mode given by

$$u(y) = \begin{cases} A(e^{q_+ y} - e^{q_- y}), & |k_x| < k_0, \quad \text{and} \quad \omega = k_x \\ 0 & \text{otherwise.} \end{cases} \quad \text{(B26)}$$

For case 2.a, the solutions are trivial due to $v(0) = 0$. For case 2.b, where $\omega = -k_x$ this condition implies

$$v(y) = \begin{cases} A(e^{r_+ y} - e^{r_- y}) & |k_x| \leqslant k_0, \\ 0 & |k_x| > k_0, \end{cases} \quad \text{(B27)}$$

and

$$u(y) = \begin{cases} A(\alpha_+ e^{r_+ y} - \alpha_- e^{r_- y}) & |k_x| \leqslant k_0, \\ Ce^{q_+ y}, & |k_x| > k_0. \end{cases} \quad \text{(B28)}$$

For $|k_x| > k_0$, the boundary condition implies $C = 0$ and for $|k_x| \leqslant k_0$ there exists a nontrivial solution only if

$$-ik_x(\alpha_+(k_x,-k_x)-\alpha_-(k_x,-k_x)) +r_+(k_x,-k_x)-r_-(k_x,-k_x)=0. \tag{B29}$$

One can check (e.g., numerically) that this equation is never satisfied for $k_x \in \mathbb{R}$. Finally, for case 3, $v(0) = 0$ implies $V_4 = -V_3$ and the membrane condition leads to

$$-ik_x(\lambda_3-\lambda_4)+(s_3-s_4)=0 \tag{B30}$$

that simplifies to

$$\frac{\epsilon k_x(s_3(k_x,\omega)+s_4(k_x,\omega))-\omega}{\omega^2-k_x^2}=0. \tag{B31}$$

One can check numerically that no edge mode appears in that case. In conclusion we only have one edge mode, as illustrated in Fig. 2(b).

c. Dirichlet/stress-free (DS). Here we impose (3c), namely $v = 0$ and $\partial_x u - \partial_y v =$ at $y = 0$. Up to a change of sign we can solve this problem based on the derivation for condition DM from the previous section. The result is plotted in Fig. 2(c). Case 1 is unchanged since $v \equiv 0$ and we have the usual Kelvin wave. Case 2 has nontrivial solution for $\omega = -k_x$ only if

$$-ik_x(\alpha_+(k_x,-k_x)-\alpha_-(k_x,-k_x))-r_+(k_x,-k_x) +r_-(k_x,-k_x)=0 \tag{B32}$$

that vanishes for two values of k_x, which are actually part of the solution of case 3. Case 3 reduces to

$$\frac{\epsilon k_x\omega(s_3(k_x,\omega)+s_4(k_x,\omega))+\omega^2-2k_x^2}{\omega^2-k_x^2}=0. \tag{B33}$$

It has a nontrivial solution with three branches: two similar to the Dirichlet/Dirichlet (no-slip) boundary condition, but that saturates at $\omega = \mp\frac{1}{\epsilon}$ when $k_x \to \pm\infty$. These branches stop in the bulk bands at $k_x = \pm k_2$ and the apparent discontinuity in Fig. 2(c) is only an artifact, cured by the two points from case 2 [see inset of Fig. 2(c)]. Finally the third branch looks like $\omega = 2k_x$ near $k_x = 0$ and stops at $k_x = \pm k_3$ when entering the bulk bands. There are no simple explicit expressions for k_2 and k_3 [in contrast to (B24)], but they can be anyway estimated numerically with arbitrary precision.

APPENDIX C: SCATTERING DATA

The scattering matrix is obtained by requiring a boundary condition on the scattering state (13) that is a superposition the bulk normal mode $\hat{\psi}_0$ (or $\hat{\psi}_\infty$) for different values of κ.

1. Bottom of the band

For the bottom of the band ω_+, we use $\hat{\psi}_0 := (\eta^0, u^0, v^0)$ (we drop the hat to simplify the notation). In the following, we denote $u^0_{\text{in}} := u^0(k_x,-\kappa)$, $u^0_{\text{out}} := u^0(k_x,\kappa)$ and $\tilde{u}^0 = u^0(k_x,\tilde{\kappa}_-(k_x,\kappa))$, where $\tilde{\kappa}_-(k_x,\kappa) = -i\sqrt{K_-}$ [see (9) and above], and similarly for v^0. The explicit expressions for u^0 and v^0 are given in (8) up to a phase multiplication by λ_0.

a. Dirichlet/Dirichlet (DD). Here we impose (3a), namely $u = v = 0$ at $y = 0$. From (13), we infer

$$\alpha u^0_{\text{in}}+\beta u^0_{\text{out}}+\gamma\tilde{u}^0=0,\quad \alpha v^0_{\text{in}}+\beta v^0_{\text{out}}+\gamma\tilde{v}^0=0, \tag{C1}$$

so that

$$S(k_x,\kappa)=\frac{v^0_{\text{in}}\tilde{u}^0-u^0_{\text{in}}\tilde{v}^0}{u^0_{\text{out}}\tilde{v}^0-v^0_{\text{out}}\tilde{u}^0}. \tag{C2}$$

The argument of S is plotted in Fig. 6(a) with respect to k_x and for several small values of κ.

b. Dirichlet/membrane (DM). Here we impose (3b), namely, $v = 0$ and $\partial_x u + \partial_y v = 0$ at $y = 0$. From (13), we infer

$$\alpha\left(k_x u^0_{\text{in}}-\kappa v^0_{\text{in}}\right)+\beta\left(k_x u^0_{\text{out}}+\kappa v^0_{\text{out}}\right)+\gamma(k_x\tilde{u}^0+\tilde{\kappa}_-\tilde{v}^0)=0,$$
$$\alpha v^0_{\text{in}}+\beta v^0_{\text{out}}+\gamma\tilde{v}^0=0, \tag{C3}$$

so that

$$S(k_x,\kappa)=-\frac{\left(k_x u^0_{\text{in}}-\kappa v^0_{\text{in}}\right)\tilde{v}^0-v^0_{\text{in}}(k_x\tilde{u}^0+\tilde{\kappa}_-\tilde{v}^0)}{\left(k_x u^0_{\text{out}}+\kappa v^0_{\text{out}}\right)\tilde{v}^0-v^0_{\text{out}}(k_x\tilde{u}^0+\tilde{\kappa}_-\tilde{v}^0)}. \tag{C4}$$

The argument of S is plotted in Figure 6(b) with respect to k_x and for several small values of κ.

c. Dirichlet/stress-free (DS). Here we impose (3c), namely, $v = 0$ and $\partial_x u - \partial_y v =$ at $y = 0$. From (13), we infer

$$\alpha\left(k_x u^0_{\text{in}}+\kappa v^0_{\text{in}}\right)+\beta\left(k_x u^0_{\text{out}}-\kappa v^0_{\text{out}}\right)+\gamma(k_x\tilde{u}^0-\tilde{\kappa}_-\tilde{v}^0)=0,$$
$$\alpha v^0_{\text{in}}+\beta v^0_{\text{out}}+\gamma\tilde{v}^0=0, \tag{C5}$$

so that

$$S(k_x,\kappa)=-\frac{\left(k_x u^0_{\text{in}}+\kappa v^0_{\text{in}}\right)\tilde{v}^0-v^0_{\text{in}}(k_x\tilde{u}^0-\tilde{\kappa}_-\tilde{v}^0)}{\left(k_x u^0_{\text{out}}-\kappa v^0_{\text{out}}\right)\tilde{v}^0-v^0_{\text{out}}(k_x\tilde{u}^0-\tilde{\kappa}_-\tilde{v}^0)}. \tag{C6}$$

The argument of S is plotted in Fig. 6(c) with respect to k_x and for several small values of κ.

2. Scattering at infinity

To explore the infinite upper limit of the band ω_+, the scattering state (13) is computed using $\hat{\psi}_\infty$ instead of $\hat{\psi}_0$ but the derivation of S is formally the same than in the previous section. Thus the expression of S in that case is given by (C2), (C4), or (C6) (respectively for DD, DM, and DS) where we replace u^0_{in}, u^0_{out} and $\tilde{u}^0$ by u^∞_{in}, u^∞_{out} and $\tilde{u}^\infty$, and similarly for v. The explicit expressions of theses quantities come from (8) up to a phase multiplication by λ_∞. The argument of S is plotted for each boundary condition in Fig. 7 with respect to k_x and for several large values of κ.

APPENDIX D: LOCAL DENSITY OF STATES

Following Ref. [78], we define the local density of states by

$$\rho(y,\omega)=\int dk_x d\kappa\,|\psi_{\text{scat}}(k_x,\kappa,y)|^2\delta(\omega-\omega_+(k_x,\kappa)) \tag{D1}$$

with $\psi_{scat}(\omega,x,y) = \psi_{\text{in}} + S\psi_{\text{out}} + T\psi_{\text{ev}}$, namely, (10) with $S = \beta/\alpha$ and $T = \gamma/\alpha$. The integration in (D1) is done for $k_x \in \mathbb{R}$ and $\kappa > 0$, but some restriction appears due to the

δ function. Indeed, $\omega = \omega_+(k_x, \kappa)$ for $\kappa = \kappa_{\text{out}}$, see (9) and above, and such solution exists only if $k_x \in [-k_{\max}, k_{\max}]$ with

$$k_{\max} = \frac{1}{\epsilon\sqrt{2}}\sqrt{-1 + 2\epsilon f + \sqrt{1 - 4\epsilon f + 4\epsilon^2\omega^2}}\,. \tag{D2}$$

Hence the change of variable in the δ-function leads to

$$\rho(y, \omega) = g(\omega)\int_{-k_{\max}}^{-k_{\max}} dk_x \frac{|\psi_{\text{scat}}(k_x, \kappa, y)|^2}{\kappa_{\text{out}}(k_x, \omega)} \tag{D3}$$

with $g(\omega) = \omega(1 - 4\epsilon f + 4\epsilon^2\omega^2)^{-1/2}$. Moreover,

$$\begin{aligned}|\psi_{\text{scat}}|^2 = |\psi_{\text{in}}|^2 + |S\psi_{\text{out}}|^2 + |T\psi_{\text{ev}}|^2 + 2\text{Re}\langle\psi_{\text{in}}, S\psi_{\text{out}}\rangle \\ + 2\text{Re}\langle\psi_{\text{in}}, T\psi_{\text{ev}}\rangle + 2\text{Re}\langle S\psi_{\text{out}}, T\psi_{\text{ev}}\rangle\end{aligned} \tag{D4}$$

with $\psi_{\text{in}} = \hat{\psi}_{\text{in}}e^{-i\kappa_{in}y}$ and $\hat{\psi}_{\text{in}} = \hat{\psi}(k_x, \kappa_{\text{in}})$, and similarly for ψ_{out} and ψ_{ev}. Since $|\psi_{\text{in}}|^2 + |S\psi_{\text{out}}|^2 = 2$, we define the free part

$$\rho_0(\omega) = g(\omega)\int_{-k_{\max}}^{-k_{\max}} dk_x \frac{|\psi_{\text{in}}|^2 + |S\psi_{\text{out}}|^2}{\kappa_{\text{out}}(k_x, \omega)}, \tag{D5}$$

independent of y. It is exactly calculable and reads after integration $\rho_0 = 2\pi g(\omega)$. Notice that $\rho_0 \sim \frac{\pi}{\epsilon}$ as $\omega \to \infty$ like free fermions in dimension two with dispersion relation $\omega \sim \epsilon k^2$. Furthermore, ρ_0 coincides with the computation of local density of state in absence of boundary. In that case, one has $\psi_{\text{scat}} = \psi_{\text{in}}$ and the integration domain is $k_x, \kappa \in \mathbb{R}^2$, leading to $\rho = \rho_0$.

Finally, the excess of density of states $\rho_1 = \rho - \rho_0$ reads as in (14) with

$$\begin{aligned}\mathcal{R}(y, k_x, \omega) = \frac{g(\omega)}{\kappa_{\text{out}}}(2\text{Re}(\langle\psi_{\text{in}}, S\psi_{\text{out}}\rangle + \langle\psi_{\text{in}}, T\psi_{\text{ev}}\rangle \\ + \langle S\psi_{\text{out}}, T\psi_{\text{ev}}\rangle) + |T\psi_{\text{ev}}|^2).\end{aligned} \tag{D6}$$

One can check that each term on the right hand side is gauge invariant, namely independent of the choice of section $\hat{\psi}$, as long as the same is taken for in, out, and ev. Thus, even though S is gauge-dependent, $\mathcal{S} = \langle\hat{\psi}_{\text{in}}, S\hat{\psi}_{\text{out}}\rangle$ is gauge invariant. Moreover, Eq. (15) follows from the fact that the winding of $\mathcal{S}$ is the same as the one for S since ψ_{in} and ψ_{out} are regular along the curve $k_x \in [-k_{\max}, k_{\max}]$ and $\omega = C^{te}$ for ω large enough (away from the edge mode branches merging with the bulk band). Such curve can be continuously deformed to the one used in Fig. 7, ending up with winding number n_∞^+. The relation (15) was also checked numerically.

APPENDIX E: REGULARIZED DIRAC HAMILTONIAN

1. Edge modes

We aim at calculating the edge modes for a semi-infinite plane $(x, y) \in \mathbb{R} \times [0, \infty]$ geometry with two different boundary conditions A and B defined in Eqs. (21a) and (21b). Following the same lines as for the shallow-water model, boundary modes are obtained as the linear combination

$$\Psi = \begin{pmatrix}A_- \\ B_-\end{pmatrix}e^{-K_- y} + \begin{pmatrix}A_+ \\ B_+\end{pmatrix}e^{-K_+ y} \tag{E1}$$

where the evanescent modes

$$\begin{pmatrix}A_\pm \\ B_\pm\end{pmatrix}e^{-K_\pm y} \tag{E2}$$

are solutions of $H_{\text{half-plane}}\Psi = E\Psi$ with

$$H_{\text{half-plane}} = \begin{pmatrix}m - \epsilon k_x^2 + \epsilon\partial_y^2 & k_x + \partial_y \\ k_x - \partial_y & -m + \epsilon k_x^2 - \epsilon\partial_y^2\end{pmatrix}. \tag{E3}$$

A direct calculation leads to

$$K_\pm = \frac{1}{\sqrt{2}\epsilon}\sqrt{2\epsilon\left(m - \epsilon k_x^2\right) + 1 \pm \sqrt{1 - 4\epsilon(m - \epsilon E^2)}}. \tag{E4}$$

Notice that, for simplicity, we have only considered the case where $\sqrt{1 - 4\epsilon(m - \epsilon E^2)}$ is real in the decomposition (E1), that is satisfied when $4|\epsilon m| < 1$. Then, defining $\lambda_\pm$ as $B_\pm = \lambda_\pm A_\pm$, one gets

$$\lambda_\pm(E, k_x) = \frac{k_x + K_\pm}{m - \epsilon k_x^2 + \epsilon K_\pm^2 + E}\,. \tag{E5}$$

Finally, inserting (E1) with (E5) into the boundary conditions A and B respectively yields

$$\text{A:}\quad \lambda_+(E, k_x) - \lambda_-(E, k_x) = 0, \tag{E6a}$$

$$\text{B:}\quad \lambda_+(E, k_x)(K_+ - k_x) - \lambda_-(E, k_x)(K_- - k_x) = 0. \tag{E6b}$$

These two implicit equations over E and k_x give the dispersion relation of the evanescent modes compatible with the corresponding boundary conditions A and B. These dispersion relations are plotted in Fig. 10.

2. Chern number

When the mass m is fixed, the regularization $\epsilon \neq 0$, allows a well defined (integer-valued) first Chern number

$$C_\pm = \frac{i}{2\pi}\int_{\mathbb{R}^2} dk_x dk_y\left(\left\langle\partial_{k_x}\psi_\pm\middle|\partial_{k_y}\psi_\pm\right\rangle - \left\langle\partial_{k_y}\psi_\pm\middle|\partial_{k_x}\psi_\pm\right\rangle\right) \tag{E7}$$

for each bulk eigenstate $\psi_\pm(k_x, k_y)$ of energy $E_\pm(k_x, k_y) = \pm\sqrt{k^2 + (m - \epsilon k^2)^2}$, solutions of (20) There are several ways to compute the Chern number. One of them consists in noticing that it coincides with the degree of the map from S^2 (the compactified $\mathbb{R}^2$ plane) to S^2 (the projective space for normalized spinors) [29]. An alternative way, that is also convenient to compute the scattering states in the following, consists in looking for the phase singularities of the normalized eigenstates $\psi_\pm(k_x, k_y)$. Indeed, $\psi_\pm(k_x, k_y)$ may have a phase singularity at $k \sim 0$ and/or at $k \sim \infty$ that can be cured locally by a gauge choice of the phase, but not necessarily removed for any point of the plane (k_x, k_y). This is a topological property of the model that is captured by the first Chern number.

In particular, the behavior of the eigenstate of positive energy

$$\hat{\psi}_+ = \frac{1}{\sqrt{2}\sqrt{E_+^2 - E_+(m - \epsilon k^2)}}\begin{pmatrix}k_x - ik_y \\ E_+ - m + \epsilon k^2\end{pmatrix} \tag{E8}$$

depends on the sign of the mass term as

$$\hat{\psi}_+ \underset{0}{\sim} \begin{cases} \begin{pmatrix} 0 \\ 1 \end{pmatrix} & \text{for } m < 0, \\ \begin{pmatrix} e^{-i\phi} \\ 0 \end{pmatrix} & \text{for } m > 0. \end{cases} \tag{E9}$$

It is regular at $k \sim 0$ when $m < 0$, but has a phase singularity when $m > 0$. This phase singularity can be removed by the gauge transformation $\psi_0 = \lambda\hat{\psi}_+$ with $\lambda = e^{i\phi} = k^{-1}(k_x + ik_y)$. Similarly

$$\hat{\psi}_+ \underset{\infty}{\sim} \begin{cases} \begin{pmatrix} e^{-i\phi} \\ 0 \end{pmatrix} & \text{for } \epsilon < 0, \\ \begin{pmatrix} 0 \\ 1 \end{pmatrix} & \text{for } \epsilon > 0, \end{cases} \tag{E10}$$

so that $\hat{\psi}_+$ is regular at $k \sim \infty$ when $\epsilon < 0$ but has the same phase singularity as at $k \sim 0$ for $\epsilon > 0$. This singularity is thus removed from $k \sim \infty$ with the same gauge transformation. The Chern number captures the impossibility to remove the phase singularity at both $k \sim 0$ and $k \sim \infty$ by the a global choice of phase. Thus it follows from (E9) and (E10) that the Chern number of the positive energy band vanishes when $\mathrm{sgn}(m) = -\mathrm{sgn}(\epsilon)$. Finally, a direct calculation leads to

$$C_\pm = \pm\frac{\mathrm{sign}(m) + \mathrm{sign}(\epsilon)}{2} \tag{E11}$$

that only takes integer values. In particular, one recovers the so-called "half-Chern number" for the usual (unregularized) massive two-dimensional Dirac equation when $\epsilon = 0$.

3. Scattering matrices

For each boundary conditions (21a) and (21b), the scattering matrix (11) is obtained at $\kappa \sim 0/\infty$ from the scattering state (10), by taking a local regular section, i.e., by choosing a local gauge such that the bulk eigenstate is singled-valued at $k \sim 0/\infty$. Focusing on ψ_+, (E9) and (E10) indicate that (E8) can be used to construct the scattering state around $k \sim 0$ when $m < 0$ and at $k \sim \infty$ when $\epsilon > 0$, while one must use $\lambda\hat{\psi}_\pm$ otherwise.

Denoting $\psi_+^i = (\phi_1^i, \phi_2^i)^T$, a smooth section of ψ_+ at $k \sim i = \{0, \infty\}$, the scattering matrices $S_i(k_x, \kappa)$ at $k \sim i$ for the band of positive energy are found to be

$$\text{A:} \quad S_i(k_x, \kappa) = \frac{\phi^i_{1,\mathrm{in}}\phi^i_{2,\mathrm{b}} - \phi^i_{2,\mathrm{in}}\phi^i_{1,\mathrm{b}}}{\phi^i_{2,\mathrm{out}}\phi^i_{1,\mathrm{b}} - \phi^i_{1,\mathrm{out}}\phi^i_{2,\mathrm{b}}}, \tag{E12a}$$

$$\text{B:} \quad S_i(k_x, \kappa) = -\frac{(k_x - |\tilde{\kappa}_-|)\phi^i_{2,\mathrm{b}}\phi^i_{1_{\mathrm{in}}} - (i\kappa + k_x)\phi^i_{1,\mathrm{b}}\phi^i_{2_{\mathrm{in}}}}{(k_x - |\tilde{\kappa}_-|)\phi^i_{2,\mathrm{b}}\phi^i_{1_{\mathrm{out}}} - (-i\kappa + k_x)\phi^i_{1,\mathrm{b}}\phi^i_{2_{\mathrm{out}}}} \tag{E12b}$$

for the boundary conditions A and B, and where

$$\tilde{\kappa}_-(k_x, \kappa) = -i\sqrt{\kappa^2 + \frac{1 - 2\epsilon\left(m - \epsilon k_x^2\right)}{\epsilon^2}}. \tag{E13}$$

Their argument is ploted as a function of k_x for different values of κ in Fig. 10. Its winding gives, in unit of 2π, the number of boundary states that enter the positive energy band by below (at finite k) or from the top (at $k \sim \infty$), so that the bulk-boundary correspondence is satisfied.

[1] M. Nakahara, *Geometry, Topology and Physics* (CRC Press, 2003).
[2] L. Onsager, Il Nuovo Cimento (1943-1954) **6**, 279 (1949).
[3] R. P. Feynman, in *Progress in Low Temperature Physics* (Elsevier, 1955), Vol. 1, pp. 17–53.
[4] *Quantized Vortex Dynamics and Superfluid Turbulence*, edited by C. F. Barenghi, R. J. Donnelly, and W. Vinen, Lecture Notes in Physics Vol. 571 (Springer Science & Business Media, 2001).
[5] J. M. Kosterlitz and D. Thouless, J. Phys. C: Solid State Phys. **5**, L124 (1972).
[6] J. M. Kosterlitz and D. J. Thouless, J. Phys. C: Solid State Phys. **6**, 1181 (1973).
[7] N. D. Mermin, Rev. Mod. Phys. **51**, 591 (1979).
[8] V. I. Arnold and B. A. Khesin, *Topological Methods in Hydrodynamics*, Applied Mathematical Sciences Vol. 125 (Springer Science & Business Media, 1998).
[9] J. F. Nye and M. V. Berry, Proc. R. Soc. A **336**, 165 (1974).
[10] Y. Hatsugai, Phys. Rev. Lett. **71**, 3697 (1993).
[11] Y. Hatsugai, Phys. Rev. B **48**, 11851 (1993).
[12] D. J. Thouless, M. Kohmoto, M. P. Nightingale, and M. den Nijs, Phys. Rev. Lett. **49**, 405 (1982).
[13] R. B. Laughlin, Phys. Rev. B **23**, 5632 (1981).
[14] B. I. Halperin, Phys. Rev. B **25**, 2185 (1982).
[15] M. Z. Hasan and C. L. Kane, Rev. Mod. Phys. **82**, 3045 (2010).
[16] Y. Hatsugai, Solid State Commun. **149**, 1061 (2009).
[17] L. Isaev, Y. H. Moon, and G. Ortiz, Phys. Rev. B **84**, 075444 (2011).
[18] P. Delplace, D. Ullmo, and G. Montambaux, Phys. Rev. B **84**, 195452 (2011).
[19] G. M. Graf and M. Porta, Commun. Math. Phys. **324**, 851 (2013).
[20] J. C. Avila, H. Schulz-Baldes, and C. Villegas-Blas, Math. Phys., Analysis Geometry **16**, 137 (2013).
[21] H. Schulz-Baldes, J. Kellendonk, and T. Richter, J. Phys. A: Math. Gen. **33**, L27 (2000).
[22] A. Elgart, G. Graf, and J. Schenker, Commun. Math. Phys. **259**, 185 (2005).
[23] E. Prodan and H. Schulz-Baldes, *Bulk and Boundary Invariants for Complex Topological Insulators,* Mathematical Physics Studies (Springer, 2016).
[24] G. M. Graf and J. Shapiro, Commun. Math. Phys. **363**, 829 (2018).
[25] M. S. Rudner, N. H. Lindner, E. Berg, and M. Levin, Phys. Rev. X **3**, 031005 (2013).
[26] J. K. Asbóth, B. Tarasinski, and P. Delplace, Phys. Rev. B **90**, 125143 (2014).
[27] G. M. Graf and C. Tauber, Annales Henri Poincaré **19**, 709 (2018).
[28] J. Shapiro and C. Tauber, Annales Henri Poincaré **20**, 1837 (2019).
[29] G. E. Volovik, Zhurnal Ehksperimental'noj i Teoreticheskoj Fiziki **94**, 123 (1988).
[30] S. Raghu and F. D. M. Haldane, Phys. Rev. A **78**, 033834 (2008).

[31] M. C. Rechtsman, J. M. Zeuner, Y. Plotnik, Y. Lumer, D. Podolsky, F. Dreisow, S. Nolte, M. Segev, and A. Szameit, Nature (London) **496**, 196 (2013).

[32] L. Lu, J. D. Joannopoulos, and M. Soljačić, Nat. Photon. **8**, 821 (2014).

[33] V. Peano, C. Brendel, M. Schmidt, and F. Marquardt, Phys. Rev. X **5**, 031011 (2015).

[34] M. G. Silveirinha, Phys. Rev. X **9**, 011037 (2019).

[35] F. Faure and B. Zhilinskii, Phys. Rev. Lett. **85**, 960 (2000).

[36] E. Prodan and C. Prodan, Phys. Rev. Lett. **103**, 248101 (2009).

[37] C. Kane and T. Lubensky, Nat. Phys. **10**, 39 (2014).

[38] R. Süsstrunk and S. D. Huber, Science **349**, 47 (2015).

[39] Z. Yang, F. Gao, X. Shi, X. Lin, Z. Gao, Y. Chong, and B. Zhang, Phys. Rev. Lett. **114**, 114301 (2015).

[40] R. Fleury, A. B. Khanikaev, and A. Alu, Nat. Commun. **7**, 11744 (2016).

[41] V. Peri, M. Serra-Garcia, R. Ilan, and S. D. Huber, Nat. Phys. **15**, 357 (2019).

[42] K. Y. Bliokh and F. Nori, Phys. Rev. Lett. **123**, 054301 (2019).

[43] M. Perrot, P. Delplace, and A. Venaille, Nat. Phys. **15**, 781 (2019).

[44] M. Perrot, P. Delplace, and A. Venaille, arXiv:1810.03328.

[45] D. Jin, L. Lu, Z. Wang, C. Fang, J. D. Joannopoulos, M. Soljačić, L. Fu, and N. X. Fang, Nat. Commun. **7**, 13486 (2016).

[46] W. Gao, B. Yang, M. Lawrence, F. Fang, B. Béri, and S. Zhang, Nat. Commun. **7**, 12435 (2016).

[47] D. Jin, Y. Xia, T. Christensen, S. Wang, K. Y. Fong, M. Freeman, G. C. Gardner, S. Fallahi, Q. Hu, Y. Wang *et al.*, Nat. Commun. **10**, 4565 (2019).

[48] M. G. Silveirinha, Phys. Rev. B **94**, 205105 (2016).

[49] K. Y. Bliokh, D. Leykam, M. Lein, and F. Nori, Nat. Commun. **10**, 580 (2019).

[50] S. Shankar, M. J. Bowick, and M. C. Marchetti, Phys. Rev. X **7**, 031039 (2017).

[51] A. Souslov, B. C. van Zuiden, D. Bartolo, and V. Vitelli, Nat. Phys. **13**, 1091 (2017).

[52] A. Souslov, K. Dasbiswas, M. Fruchart, S. Vaikuntanathan, and V. Vitelli, Phys. Rev. Lett. **122**, 128001 (2019).

[53] C. Tauber, P. Delplace, and A. Venaille, J. Fluid Mech. **868** (2019).

[54] T. Van Mechelen and Z. Jacob, Phys. Rev. A **98**, 023842 (2018).

[55] K. Iga, J. Fluid Mech. **294**, 367 (1995).

[56] J. Li, A. F. Morpurgo, M. Büttiker, and I. Martin, Phys. Rev. B **82**, 245404 (2010).

[57] K. Iga, Fluid Dynamics Res. **28**, 465 (2001).

[58] D. Meidan, T. Micklitz, and P. W. Brouwer, Phys. Rev. B **84**, 195410 (2011).

[59] I. C. Fulga, F. Hassler, A. R. Akhmerov, and C. W. J. Beenakker, Phys. Rev. B **83**, 155429 (2011).

[60] I. C. Fulga, F. Hassler, and A. R. Akhmerov, Phys. Rev. B **85**, 165409 (2012).

[61] W. Hu, J. C. Pillay, K. Wu, M. Pasek, P. P. Shum, and Y. D. Chong, Phys. Rev. X **5**, 011012 (2015).

[62] G. Bal, arXiv:1709.00605.

[63] C. L. Fefferman, J. P. Lee-Thorp, and M. I. Weinstein, Annal. PDE **2**, 12 (2016).

[64] G. Bal, J. Math. Phys. **60**, 081506 (2019).

[65] F. Faure, arXiv:1901.10592.

[66] A. Drouot, arXiv:1901.06281.

[67] J. Avron, J. Stat. Phys. **92**, 543 (1998).

[68] S. Ganeshan and A. G. Abanov, Phys. Rev. Fluids **2**, 094101 (2017).

[69] Edge numbers n_{top} and n_{bottom} are defined up to a global sign, depending on the orientation of the boundary, but the relative sign between them in their definition persists anyway.

[70] P. Dedalus, http://ascl.net/1603.015 (2016), http://dedalus-project.org.

[71] K. J. Burns, G. M. Vasil, J. S. Oishi, D. Lecoanet, and B. P. Brown, arXiv:1905.10388.

[72] Y. Avishai and Y. B. Band, Phys. Rev. B **32**, 2674(R) (1985).

[73] W. Thomson, Proc. R. Soc. Edinburgh **10**, 92 (1880).

[74] F. Faure and B. Zhilinskii, Lett. Math. Phys. **55**, 219 (2001).

[75] T. Fukui, K. Shiozaki, T. Fujiwara, and S. Fujimoto, J. Phys. Soc. Jpn. **81**, 114602 (2012).

[76] R. Dashen, S.-k. Ma, and H. J. Bernstein, Phys. Rev. **187**, 345 (1969).

[77] V. Gasparian, T. Christen, and M. Büttiker, Phys. Rev. A **54**, 4022 (1996).

[78] S. Souma and A. Suzuki, Phys. Rev. B **65**, 115307 (2002).